Investigating the Impact of Biochemical and Mechanical Stimuli on Motor Neuron Growth

by

Angel Bu

B.S. Biomedical Engineering
University of Florida 2021

Submitted to the Department of Mechanical Engineering in partial fulfillment of the requirements for the degree(s) of

Master of Science

at the

Massachusetts Institute of Technology

June 2023

Authored by: Angel Bu
Department of Mechanical Engineering
May 12th, 2023

Certified by: Ritu Raman
Department of Mechanical Engineering

Accepted by: Nicolas Hadjiconstantinou
Chairman, Committee on Graduate Students

Investigating the Impact of Biochemical and Mechanical Stimuli on Motor Neuron Growth

by

Angel Bu

Submitted to the Department of Mechanical Engineering on May 12th, 2023 in Partial Fulfillment of the Requirements for the Degree of Master of Science

ABSTRACT

Peripheral nerve injuries are one of the most prevalent trauma injuries, and the current golden standard for treatment is an autologous nerve graft. The use of tissue engineered nerve grafts has increased in recent years, a neural scaffold, cellular or acellular, is utilized to promote nerve repair. Prior research has shown that transcutaneous optogenetic stimulation on grafted engineered tissue can promote reinnervation and angiogenesis in a rat volumetric muscle loss model. Our study queried the individual effects of biochemical and mechanical stimuli on neuronal growth to push the field of neuromuscular systems forward. We utilized optogenetic stimulation to emulate the biochemical effects and a magnetic fibrin platform to isolate the mechanical effect. To develop our magnetically actuatable substrate we optimized a fibrin hydrogel that would have a similar stiffness to skeletal muscle. Then, we added rectangular segments of 1:10 PDMS with 25% v/v 4-micron iron microparticles. These rectangular segments within the fibrin hydrogel were then cyclically actuated by a permanent neodymium magnet. Our results showed a substantial increase in neurite outgrowth in the experimental group which was supplemented with exercised media from an optogenetic muscle monolayer. The isolated biochemical effect was a substantial increase in the rate of neurite growth between the groups. In our preliminary neuromuscular system, we saw a degree of co-localized alignment between the neurites and differentiated muscle. This neuromuscular protocol seems to have physiological alignment similarities to in vivo tissue. We quantified alignment through a Fast Fourier Transform of the image data of the separate imaging channels, RFP for muscle and GFP for motor neuron. Finally, our magnetic fibrin platform found no significant increase in myofiber length and width when mechanical stimulation was applied after myoblast differentiation. In future research, we are exploring the biochemical and magnetic stimulation on our neuromuscular co-culture and actuate the myoblasts at an earlier cellular stage to impact alignment. In conclusion, our studies found that stimulated media aids in neurite outgrowth. In future research, we will perform RNA-Seq on our systems to verify the specific biological pathways and upregulated growth factors.

Thesis supervisor: Dr. Ritu Raman

Title: d'Arbeloff Career Development Assistant Professor of Mechanical Engineering

Table of Contents

ABSTRACT 2
1. Introduction 5
1.1 General Overview of Neuromuscular Co-Culture 5
1.1.1 Current State of In Vitro 3D Neuromuscular Systems 6
1.1.2 Stem Cell Sources for Neuronal Culture 7
1.1.3 Neurons as a Control System in Biological Robots 8
1.2 Presence of Neurotrophic Factors 8
2. Experimental Design 9
2.1 Cell Culture Parameters and Optimization 11
2.1.1 Neuron Differentiation and Culture 11
2.1.2 Muscle Differentiation and Culture 12
2.1.3 Neuromuscular Assembly 13
2.2 Mechanisms of Actuation 14
2.2.1 Optogenetic Stimulation 14
2.2.2 Macroscale Magneto-Mechanical Stimulation 15
2.2.2.1 Development of Magnetically Actuated Fibrin Hydrogel 15
2.2.2.2 Optimization Parameters for Magnetic Platform 16
3. Results 18
3.1 Preliminary Results of Neuromuscular Culture 18
3.2 Biochemical Impact of Exercised Media on Neuron Monoculture 18
3.3 Neurite Alignment with Differentiated Muscle 19
3.4 Impact of Magnetic Stimulation on Differentiated Myofibers 20
4. Discussion and Conclusions 22
5. References 24

List of Figures

Figure 1-1: 3D-Neuromuscular biobots 7

Figure 1-2: Phosphoproteomic heatmap of exercised *in vivo* grafted tissue 9

Figure 2-1: Characterization of 2D protocol and timeline 10

Figure 2-2: GFP expression with time in GFP::HB9 HBG3 stem cells 12

Figure 2-3: Light meter data of our LED setup 14

Figure 2-4: Characterization of the magnetic stimulation platform 16

Figure 2-5: Displacement data of our magnetic substrate 17

Figure 3-1: Progression of novel neuromuscular co-culture fabrication 18

Figure 3-2: Biochemical effects on neuron monoculture's neurite outgrowth 19

Figure 3-3: FFT alignment of co-localized neuromuscular tissue 20

Figure 3-4: Experimental timeline of our magnetic stimulation 21

Figure 3-5: Myofiber length and width during magnetic stimulation 22

1. Introduction

Peripheral nerve injuries are one of the most prevalent injuries seen in approximately, 2.8% of trauma patients[1]. This demonstrates a growing need for alternative therapies and treatment options for individuals with peripheral nerve injuries. The golden standard for axonotmesis and neurotmesis injuries, which lead to loss of function and Wallerian degeneration is an autologous nerve graft[2]. This option is not always readily available due to the nature of the procedure. Producing an injury at the donor site may result in positive outcomes for nerve regeneration, but the donor site can suffer from long-term effects including decreased sensation, cold sensitivity, pain, and functional impairment[3,4].

The use of tissue engineered nerve grafts has increased in recent years, a neural scaffold, cellular or acellular, is loaded with growth factors to be able to replicate the efficacy of autologous nerve grafts[5]. As the development of tissue engineered nerve grafts progresses so does the potential for a better alternative in peripheral nerve repair[2,6]. Our study queried the individual effects of biochemical and mechanical stimuli on neuronal growth to push the field of neuromuscular systems forward for applications such as tissue-engineered nerve grafts.

1.1 General Overview of Neuromuscular Co-Culture

A neuromuscular co-culture traditionally comprises a neuronal component, most commonly differentiated from a stem cell, and a muscle component, harvested directly from a patient or differentiated from a myoblast. Neuromuscular co-cultures can also

contain support cells created from the neural stem cells such as Schwann and satellite cells[7].

1.1.1 Current State of In Vitro 3D Neuromuscular Systems

Many researchers have been able to create organ-on-a-chip neuromuscular systems. Among those models a few studies stand out, such as Osaki et al. (2020) they created a standardized method of producing organ-on-a-chip neuromuscular junctions[8]. This model was used to test drug screening efficacy in an amyotrophic lateral sclerosis disease model measuring functional metrics such as muscle force and neurite elongation speed[9].

Moreover, the implementation of neuromuscular systems in modular 3D cultures has been established for quite some time, Cvetkovic et al. (2017) developed a similar bio-bot to which our group manufactures but contains a layer of motor neuron embryoid bodies(EBs)[10]. Following this study, other groups produced similar systems demonstrating the reproducibility of neuromuscular junctions in vitro[11]. Our Raman group has historically created biobots and neuromuscular biobots and managed to recreate this system with our polydimethylsiloxane(PDMS) molds, Figure 1-1.

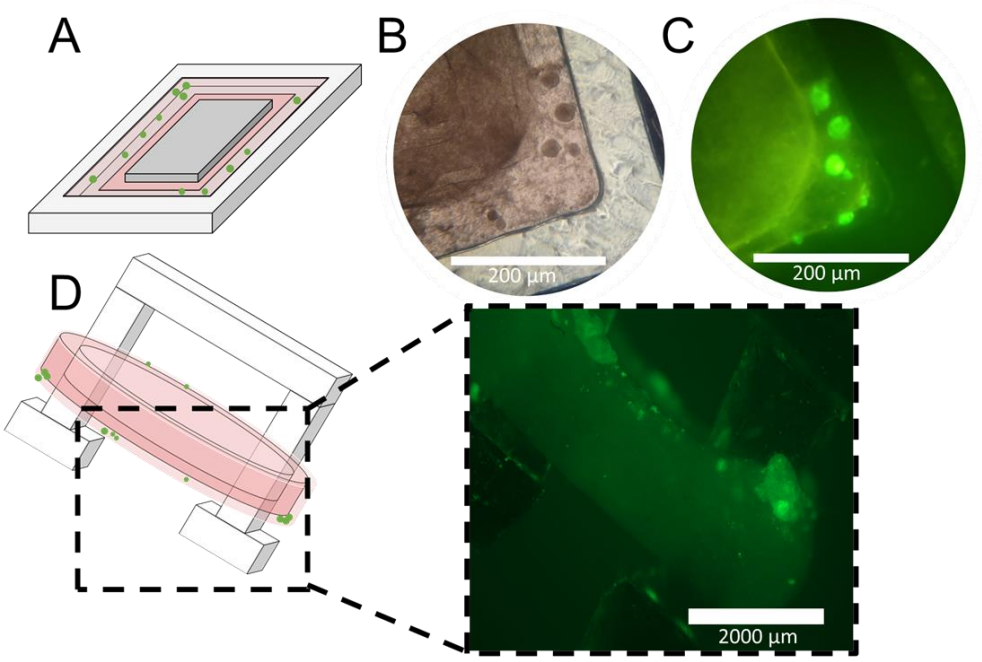

Figure 1-1: (A) Characterization of the PDMS mold and EBs within the second layer. (B) Phase contrast and (C) fluorescent image of the murine HB9::GFP fluorescent HBG3 EBs within a fibrin matrix seeded with C2C12 myoblasts. (D) Neuromuscular rings transferred onto our PDMS skeletons mimic muscle-tendon behavior in an in vitro culture.

1.1.2 Stem Cell Sources for Neuronal Culture

Stem cells contain an innate cellular plasticity that enables them to reconfigure into a multitude of cell types[12]. With regard to neuron differentiation, stem cells are an efficient way to produce neural stem cells from a variety of sources, this includes adipose-derived stem cells, embryonic stem cells, and induced pluripotent stem cells[8,13,14]. The latter, induced pluripotent stem cells, are a target for neuron-related disease modeling due to their ability to recreate genetic mutations in vitro[15]. The variety of sources for neural stem cells has exponentially increased the research in the field and expanded upon the information that can be gleaned from each model[16–18].

1.1.3 Neurons as a Control System in Biological Robots

Neurons are autologous to the controller in a mechanical system, they can be used to modulate force in the musculoskeletal system and this analogy has been reproduced in vitro. Aydin et al. (2019) utilized an optogenetic neurosphere to produce motile bots driven by optical stimulation[19]. This design cleverly showed the possibility of engineering biological constructs from a robotics viewpoint. Moreover, Webster et al. (2017) took a different approach and directly harvested these neuromuscular tissues to be used in a 3D-printed body[20]. The tissue was then chemically stimulated using carbamylcholine chloride, carbachol, a known neurotransmitter that mimics the effect of acetylcholine in nicotinic and muscarinic receptors[20].

1.2 Presence of Neurotrophic Factors

In Rousseau et al. (2023), we investigated the effect of exercised muscle through a phosphoproteomic analysis. As seen in Figure 1-2, the data demonstrated an upregulation of phosphorylated peptides in cluster 5 for the exercised group. Cluster 5 contained peptides crucial to axonogenesis and angiogenesis. This is the cornerstone for further investigation into the biochemical pathways that promote axonal growth during muscular contraction. These results also reinforced the idea that the native rat tissue innervated our grafted muscle with the help of optogenetic stimulation[21].

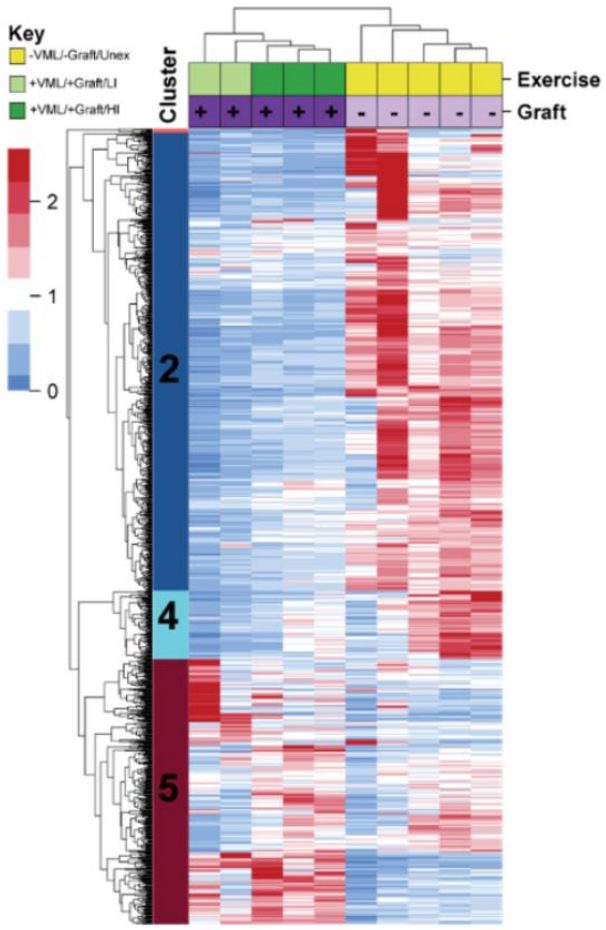

Figure 1-2: Hierarchical clustering of tyrosine phosphorylated peptides from +VML/+Graft/+LI, +VML/+Graft/HI, and control (-VML/-Graft).

2. Experimental Design

We designed a study that isolates the individual effects of both biochemical and mechanical stimulation on neurite outgrowth, Figure 2-1. To culture differentiated muscle long-term in vitro, we seeded a glass bottom plate(Cellvis, Mountain View, CA, USA) with a fibrin hydrogel that would serve as a deformable substrate to exercise muscle. The fibrin hydrogel consists of 20 mg of fibrinogen(F8630, MilliporeSigma) to 1 Unit of thrombin(T4648, MilliporeSigma). We utilized optogenetic C2C12s to create exercised media for our biochemical effect. Furthermore, we optimized a macroscale magneto-

mechanical stimulation setup within our fibrin hydrogel for isolating mechanical stimulation.

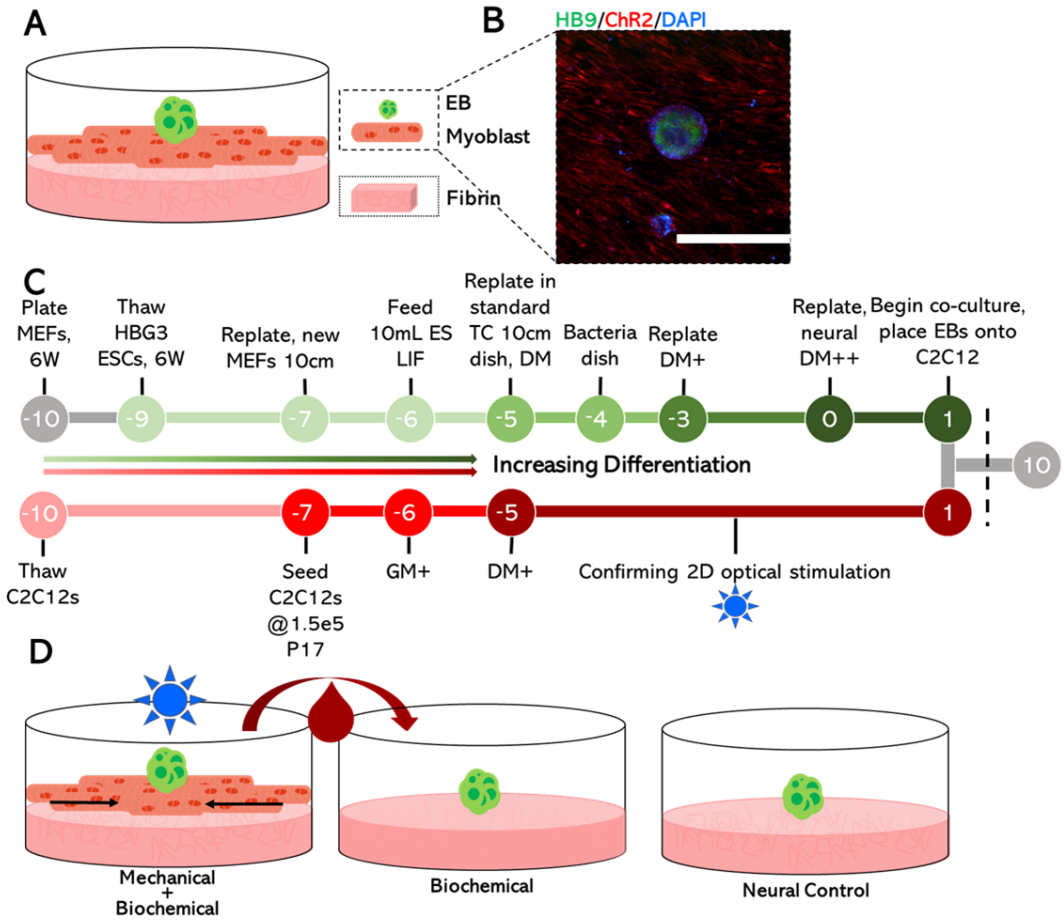

Figure 2-1: (A) Characterization of neuromuscular co-culture with a (B) fluorescent image demonstrating the HB9::GFP, Chr2-TdTomato, and DAPI on day 1 of co-culture. (C) The cell culture timeline is also shown leading up to the neural and myogenic differentiation. (D) Characterization of the different conditions that isolate the mechanical and biochemical effects.

2.1 Cell Culture Parameters and Optimization

2.1.1 Neuron Differentiation and Culture

The HBG3 HB9::GFP embryonic stem cells were cultured and expanded into EBs. On day -5, the EBs were differentiated with a base formulation of 50%(v/v) Neurobasal(21103049, Thermofisher Scientific, Waltham, MA, USA) and 50%(v/v) Advanced DMEM/F12(12634028, Thermofisher Scientific), supplemented with 10%(v/v) KnockOut Serum Replacement(10828010, Thermofisher Scientific), 1%(5000U/mL) penicillin-streptomycin(15070063, Thermofisher Scientific), 1%(v/v) L-glutamine(A2916801, Thermofisher Scientific), and 0.1mM β-mercaptoethanol(21985023, Thermofisher Scientific). On day -3 the neural differentiation media was supplemented with 1µM of purmorphamine(540220, MilliporeSigma) and retinoic acid(R2625, MilliporeSigma). In the final days of differentiation, day 0, 10ng/mL of glial-derived neurotrophic factor(PR27022, Neuromics, Edina, MN, USA) and ciliary neurotrophic factor(C3710, MilliporeSigma) were added. The HB9::GFP genetically modified stem cells express the green fluorescent protein as it matures into a motor neuron lineage, this was our quality control marker before implantation of the EBs into the co-culture[22], Figure 2-2.

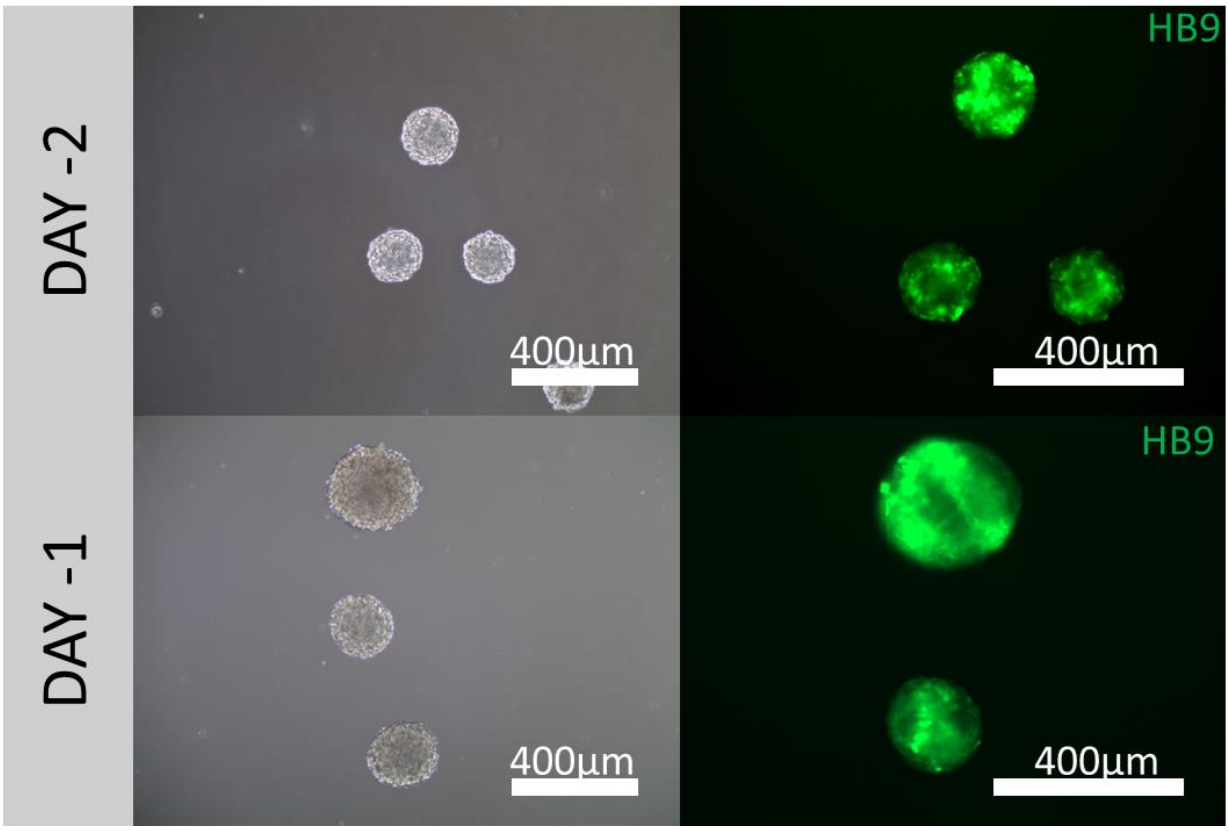

Figure 2-2: Progression of HB9::GFP HBG3 embryonic stem cells into motor neuron embryoid bodies.

2.1.2 Muscle Differentiation and Culture

The Channelrhodopsin-2(Chr2) modified C2C12 myoblasts were cultured and expanded in muscle growth media, DMEM with 4.5 g/L glucose, L-glutamine, and sodium pyruvate(10013CV, Thermofisher Scientific) with 10% fetal bovine serum(F2442, MilliporeSigma) and 1% L-glutamine(A2916801, Thermofisher Scientific) and penicillin-streptomycin(MT30002CI, Thermofisher Scientific). During muscle seeding 1mg/mL of aminocaproic acid(A2504, MilliporeSigma) was added to the media to create muscle growth media plus. After a day of seeding the cells into the fibrin hydrogel, the media was swapped to muscle differentiation media plus which is made up of DMEM with 4.5 g/L glucose, L-glutamine, and sodium pyruvate(10013CV, Thermofisher Scientific) with 10%

horse serum(26050070, Thermofisher Scientific), 1% L-glutamine(A2916801, Thermofisher Scientific), 1% penicillin-streptomycin(MT30002CI, Thermofisher Scientific), 1mg/mL of aminocaproic acid(A2504, MilliporeSigma), and 50 ng/mL of insulin-like growth factor-1(I1146, Millipore Sigma).

2.1.3 Neuromuscular Assembly

The assembly of the neuromuscular culture starts with constructing the fibrin hydrogel the day before seeding the C2C12 ChR2 myoblasts. After one day on growth media plus and five subsequent days on muscle differentiation media plus, the muscle monolayer has fused into multinucleated myofibrils. At that point they have become contractile and are sensitive to 440 nm wavelength light. The EBs which should be fully fluorescent are now implanted onto the 2D muscle monolayer. The co-culture media is a complete neural differentiation media, neurotrophic factors included, with 10% horse serum, 1 mg/mL of aminocaproic acid, and 50 ng/mL of recombinant IGF-1. For initial seeding, growth factor reduced Matrigel®(354230, Corning®, Corning, NY, USA) was diluted into the media at a concentration of 1:1000. After 24 hours, the media was changed back to before the dilution of the Matrigel®.

We have also attempted a novel method of neuromuscular assembly by taking advantage of the EBs' ability to lay down support extracellular matrix. This involves establishing a neuronal boundary around the EB monoculture and then seeding the myoblasts to differentiate for 3 days around the neuronal extracellular matrix. This approach separates the two electrically active soma and helps us determine if the neurite alignment shifts after muscle layer differentiation.

2.2 Mechanisms of Actuation

To isolate the mechanical effects from the biochemical effects of muscle exercise we had to develop a method of external physical actuation. The use of optogenetic muscle stimulation inadvertently upregulates the use of neurotrophic factors[21].

2.2.1 Optogenetic Stimulation

Optogenetic stimulation occurs through the blue-light sensitive cation channel, Channelrhodopsin-2, in the genetically engineered cell membrane of our C2C12 myoblasts. Our stimulation setup utilized two 5W blue light bulbs to flood the 24-well plate dish with blue light. Using a MOSFET and function generator we were able to control the frequency, duty cycle, and wave type. Each optical stimulation cycle was 30 minutes of 1Hz, 20% duty cycle. The optical power meter data(PM100D/S130C, ThorLabs, Newton, NJ, USA) demonstrated more than sufficient light intensity in the 8 wells of interest in the center of a 24-well plate to confirm activation of the blue-light sensitive Channelrhodopsin-2, Figure 2-3.

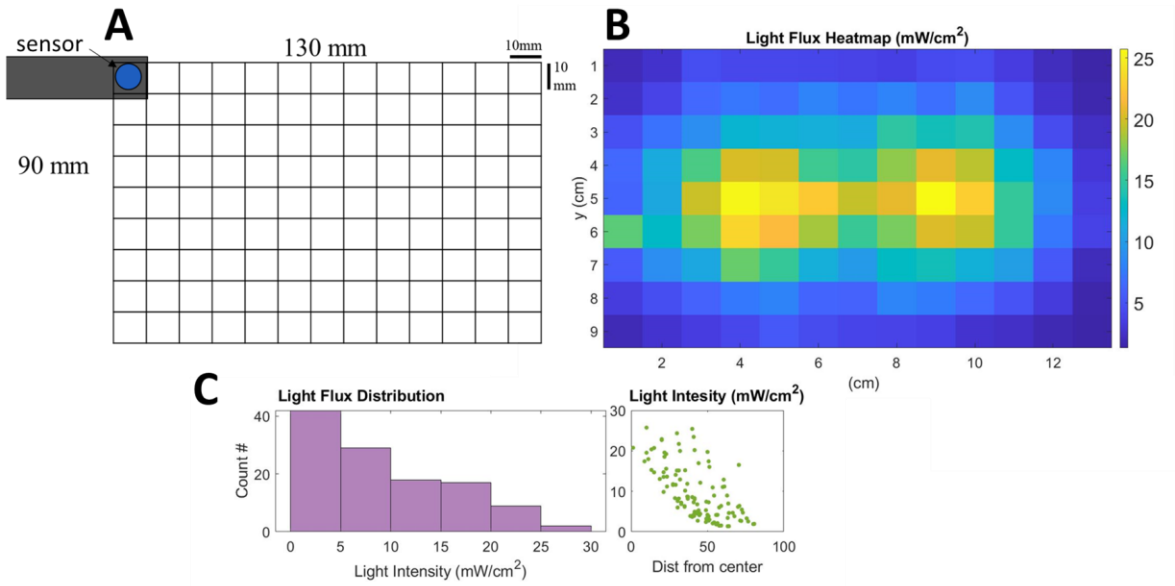

Figure 2-3: Analysis of our custom light stimulation setup. (A) The area for optical power meter analysis was segmented into 10mm x 10mm squares to fit the sensor aperture area of 9.5 mm diameter, the total approximate area is based on the size of a standard well plate. The power meter was exclusively recording power for. (B) Light flux heatmap is shown after averaging n=10 recordings for each square. (C) The light flux distribution histogram is then plotted alongside the light intensity as a function of its displacement from the center of the 24-well plate.

2.2.2 Macroscale Magneto-Mechanical Stimulation

2.2.2.1 Development of Magnetically Actuated Fibrin Hydrogel

To isolate the mechanical effects, we developed a platform that could apply external force onto our muscle monolayer. This was done by inserting 1:10 PDMS prisms into our fibrin hydrogel with 25% w/v iron microparticles, 4 μm diameter spheres, carbonyl iron. When we apply a moving magnetic field to the fibrin hydrogel with the magnetic PDMS within it, resulting in a local deformation of the substrate surrounding the PDMS, Figure 2-4.

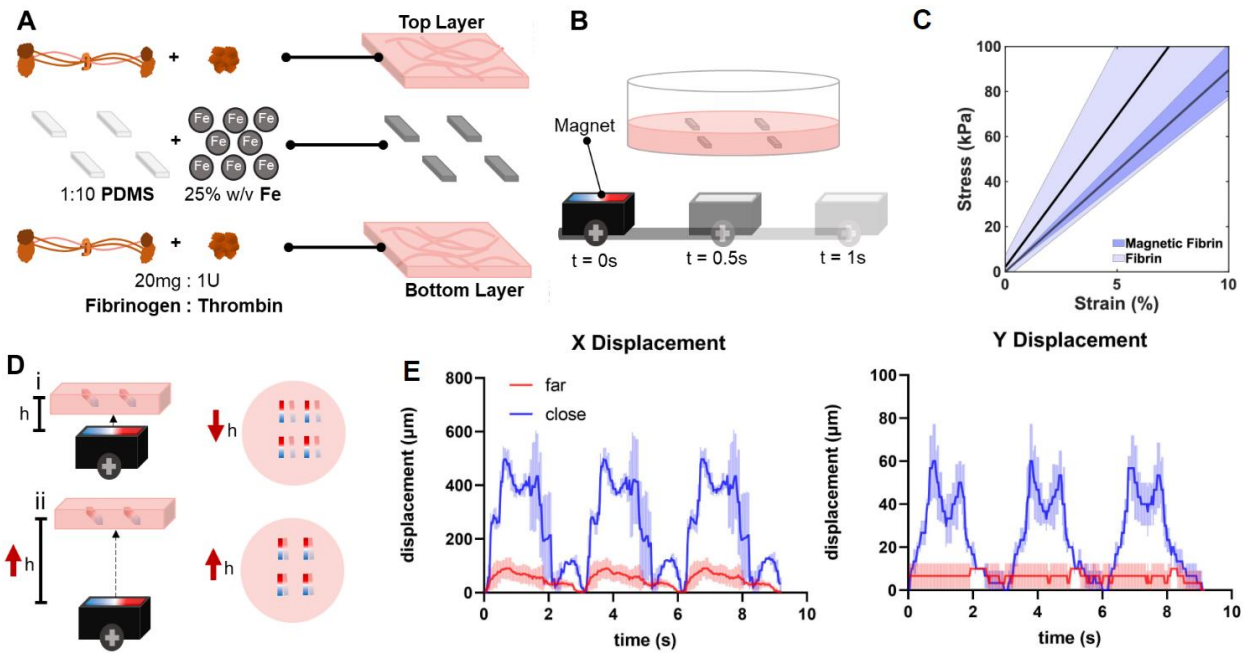

Figure 2-4: (A) Fabrication process of our magnetic fibrin platform and (B) timing of our magnet beneath our substrate. (C) The stress-strain curve of the magnetic fibrin is plotted alongside the regular fibrin substrate. (D) Diagram showing the relationship between the displacement of the permanent magnet and the total movement of the substrate's surface, this is (E) quantified by plotting displacement versus time.

2.2.2.2 Optimization Parameters for Magnetic Platform

Initial work on the magnetic platform was done by inserting 15 μm polystyrene beads(FluoSpheres, Invitrogen, Waltham, MA, USA) that contain green fluorescence to easily track the substrate displacement, Figure 2-5. The bead displacement was then tracked through ImageJ(National Institute of Health, Bethesda, MD, USA) using the TrackMate plugin. We found similar amounts of displacement caused by permanent magnet deformation when compared to optically stimulated differentiated muscle from our 2D platform. Future work on this magnetic platform involves 3D printing the iron

loaded PDMS onto the fibrin in aligned rows to maximize the torsional displacement around each iron strip.

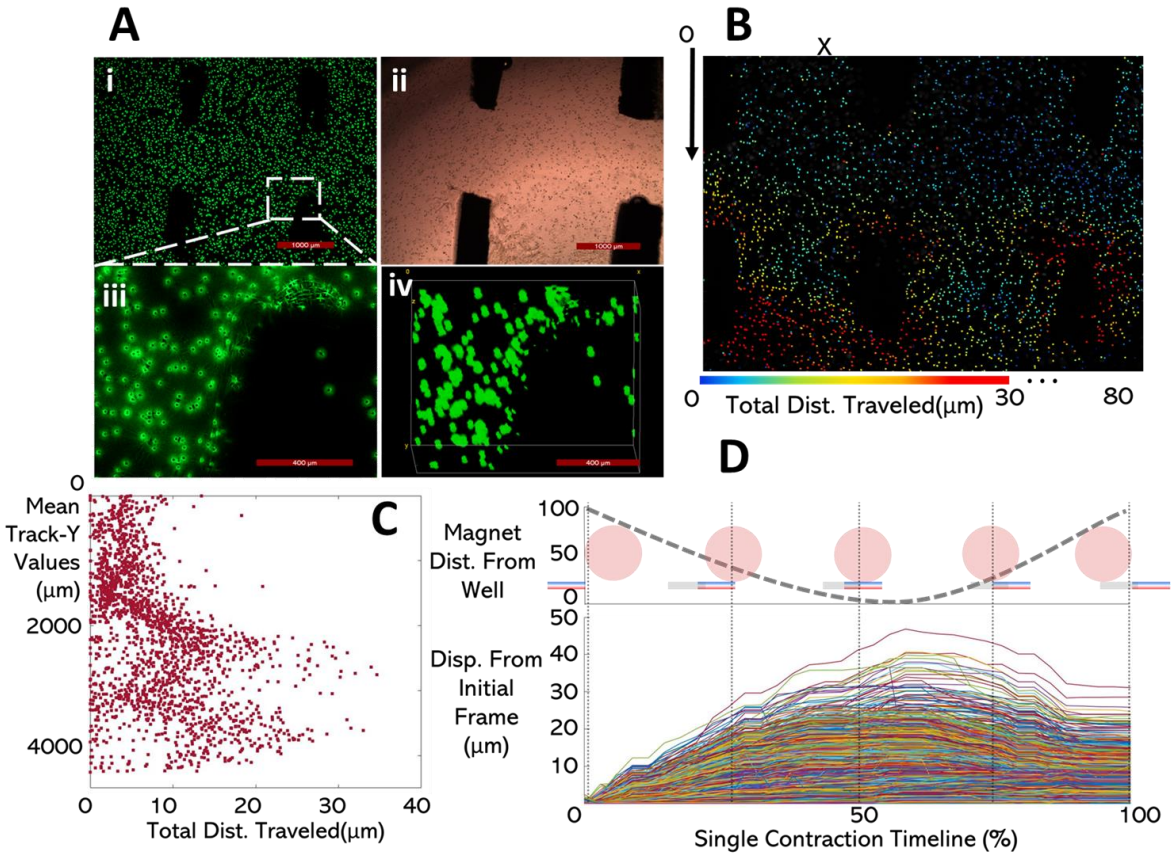

Figure 2-5: (A)(i) Fluorescent z-stack image of 2nd fibrin layer containing green fluorescent 15 μm polystyrene beads to track substrate movement, and an adjacent close-up image (iii). (ii) Phase contrast image of the 2nd fibrin layer with fluorescent beads. (iv) Volumetric projection of the fluorescent polystyrene spheres demonstrates depth into the fibrin gel and uniform movement in the z-direction. (B) TrackMate output for bead tracking. (C) Total distance traveled plotted against the average Y values of each bead during movement. (D) Method of actuation shown above all track displacements during a single magnetic contraction.

3. Results

3.1 Preliminary Results of Neuromuscular Culture

Utilizing our novel method of creating neuromuscular co-cultures, the EB physically separates itself from the muscle monolayer using its extracellular matrix. As shown in Figure 3-1, the phase contrast image demonstrates which parts of the EB and its extracellular matrix express the GFP seen in motor neuron differentiation. The surrounding matrix around the EB is not fluorescing but is seen prior to the seeding of the C2C12 myoblasts. The myoblast begins to fuse and becomes confluent around five days post-seeding of the C2C12s, this metric can be adjusted by seeding at a higher density.

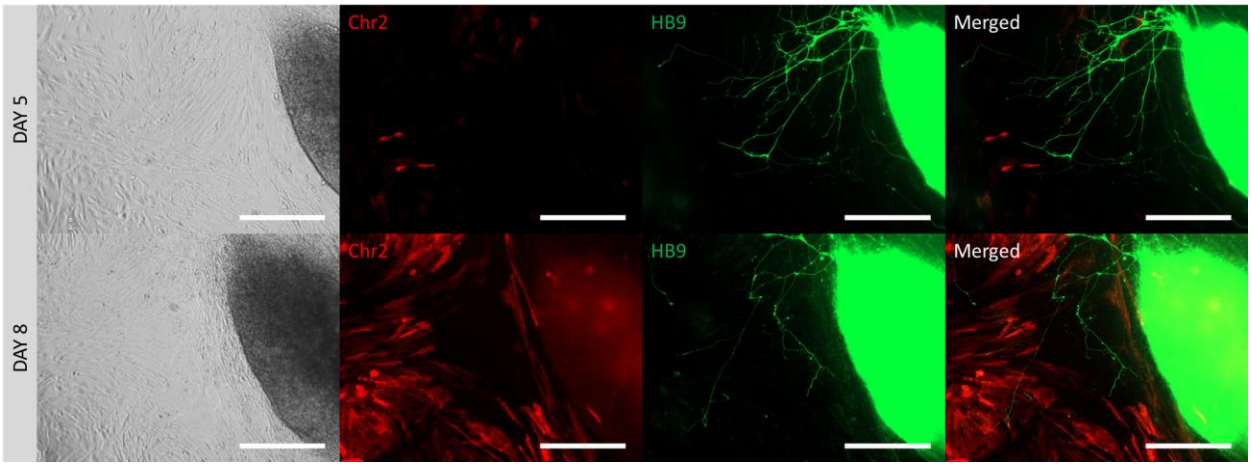

Figure 3-1: (Top Row) Phase contrast and fluorescent images of our neuromuscular co-culture on day 5, two days after the seeding of our genetically engineered ChR2-tdTomato C2C12 myoblasts. (Bottom Row) Same imaging area shown on day 8, all scale bars shown are 400 µm.

3.2 Biochemical Impact of Exercised Media on Neuron Monoculture

As seen in Figure 3-2, there is a substantial increase in neurite density and length when we compared the supplemented group to the control group. This can also be seen in Figure 3-2C, there is an increase in total neurite length and rate of axon growth in the

supplemented group. Furthermore, there is a similar linear relationship between neurite length and time. The difference in slope of these linear relationships is described by Figure 3-2B which demonstrates an increase in total neurite length growth rate in the supplemented group by almost double the rate of the control group.

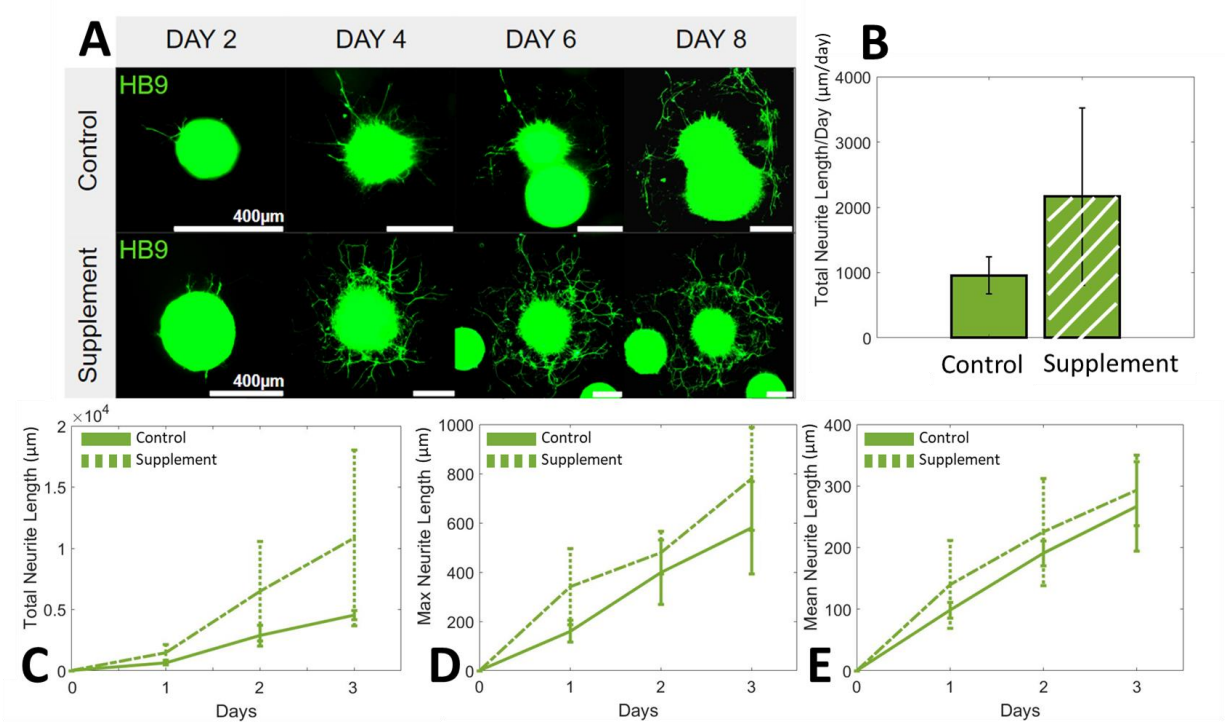

Figure 3-2: (A) Representative images for neuron monoculture shown for both control and supplemented groups. The plots show (B) total neurite length slope across the two groups and line plots for (C) total neurite length, (D) max neurite length, and (E) mean neurite length across time, error bars demonstrate standard deviation, n=3.

3.3 Neurite Alignment with Differentiated Muscle

The neurites extending into the locally aligned muscle seem to show preferential alignment towards the direction of tension in the differentiated muscle, Figure 3-3. As seen in Figure 3-3, the channels were separated to isolate the alignment of both ChR2-tdTomato and HB9::GFP. The intensity data shows local alignment around the

differentiated muscle fiber. In Figure 3-3C, the two lines track almost identically, the RFP signal has noise about the 0° and 90° radial sum, despite the noise the rest the signal intensity sections are similar.

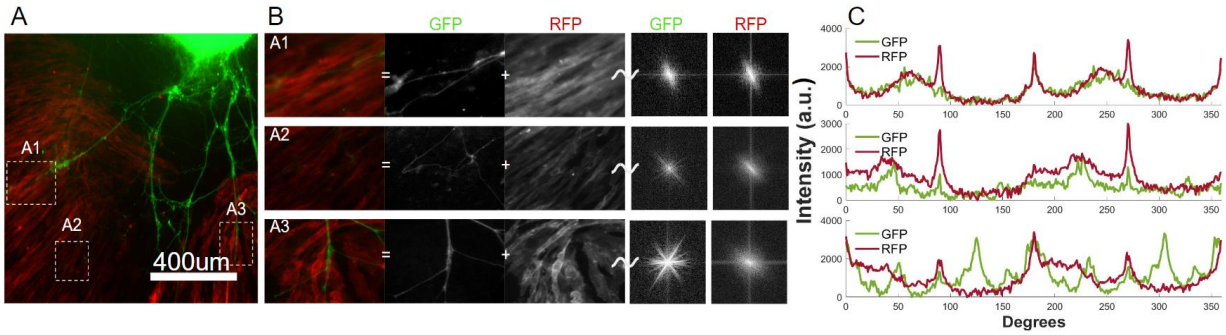

Figure 3-3: (A) A fluorescent image of a neuromuscular co-culture with (B) regions isolating both the GFP and RFP signal. (C) The intensity of the FFT for each fluorescent signal is then calculated as a radial sum for 360 degrees and plotted together.

3.4 Impact of Magnetic Stimulation on Differentiated Myofibers

The impact of 30 minutes of 1Hz magnetic stimulation on the muscle layer for ten days after muscle differentiation and fusion had minimal effect on the alignment of the muscle on the last day of magnetic stimulation. After performing an FFT on the sections of muscle surrounding the magnetic PDMS, the data was averaged for each quadrant of an image or sample, Figure 3-4. Using the directionality plugin in ImageJ, a Gaussian fit is applied onto the intensity histogram to determine the direction of the FFT signal and the dispersion, Figure 3-4. There is a slight trend in the data that suggests that the dispersion of the experimental group was much lower than the control. This means that the FFT alignment was much more like one another in the experimental than the control group. We analyzed the data using this method to describe global alignment with respect to the different regions of the differentiated myofibers and to show how consistent the

alignment would remain with applied external stimulation. A Student t-test did not find significance in any of the metrics except between the standard deviation of the experimental and control groups for the dispersion's standard deviation control (mean±s.d.,5.23±2.14) and experimental (3.04±1.66) conditions (t=3.73,df=3,p=0.034,CI = [0.32 4.06]).

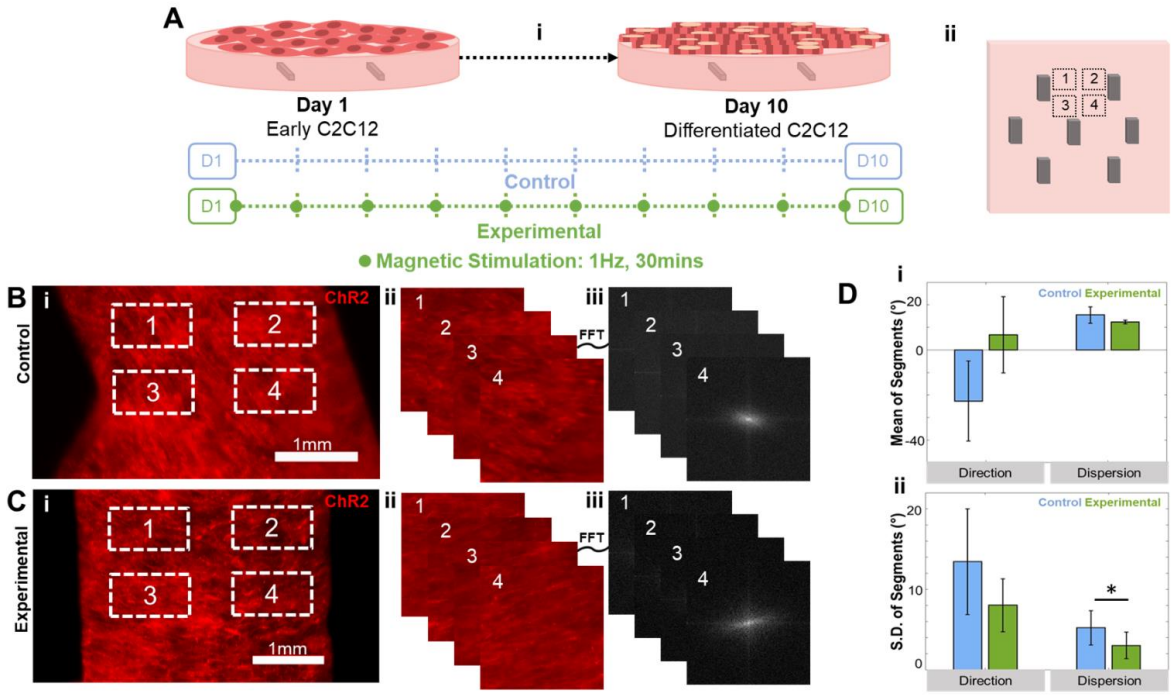

Figure 3-4: (A) (i)Experimental timeline for the control and magnetically stimulated group alongside with (ii) the imaging area criteria for each well, n=4. The RFP images were segmented into four sections and the FFT data was averaged for (B) control and (C) experimental groups. (D) The (i) mean and (ii) standard deviation of the four segments' direction and dispersion was averaged across each group, *p<0.05.

With respect to the length and width of the muscle fibers, we found no significant differences between the control and experimental groups on day 5 and day 8 of stimulation Figure 3-5. Although, the data shows a substantial increase in length and

width of myofibers with time. A Student t-test showed significance between the days in the same group but not across groups on the same day, Figure 3-5.

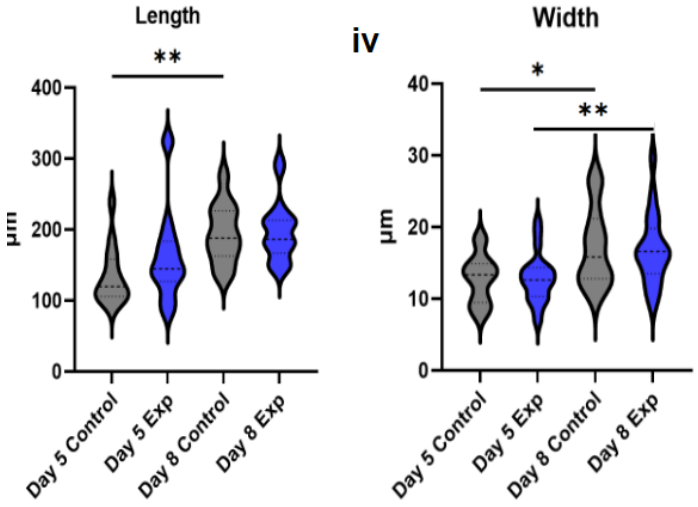

Figure 3-5: (Left) Myofiber length is shown as a violin plot for day 5 control and experimental versus day 8. (Right) Myofiber width is shown as a violin plot for day 5 control and experimental versus day 8, *p<0.05,**p<0.01.

4. Discussion and Conclusions

The in vitro data reaffirms what we saw during the in vivo data in the volumetric muscle loss graft data. The phosphoproteomic data in Rousseau et al. (2023) demonstrated an upregulation of phospho-tyrosine driven integrin and angiogenesis signaling in optogenetically exercised muscle[21]. This led us to believe that replicating this experiment in vitro would impact neurite outgrowth. We went about doing this by exercising media in optogenetic muscle and then supplementing that media into our neuron monoculture and comparing the control and experimental groups. We found a substantial increase in max neurite length and migration in the supplemented exercised media group than the control. This may be occurring through the expression of neurotrophic factors produced by the exercised muscle which is then supplemented into

the neuron monoculture. Future research involves querying the impact of exercising optogenetic muscle versus no exercise on our optimized neuromuscular co-culture. In addition, we plan on conducting RNA-Seq to verify further the impact of exercise on the transcriptomes of our in vitro experiments. As for the mechanical impact, we plan on applying our magnetic stimulation on a neuron monoculture and then our optimized neuromuscular co-culture to determine not only if mechanical stimulation impacts neurite growth but al the presence of neuron-muscle contact. We also plan on staining for α-bungarotoxin to characterize the development of neuromuscular junction and leveraging the use of advanced imaging techniques, such as scanning electron microscopy, to better visualize our data. An interesting observation is that our EBs developed an extracellular matrix that does not contain GFP or motor neuron lineage, but shows cell morphology similar to that of fibroblasts or confluent myoblasts. We believe these to be glial support cells produced by the mostly differentiated embryonic stem cell motor neuron sphere.

Preliminary results with our optimized neuromuscular protocol show a local alignment of the differentiated myofibers but a lack of global alignment. There is a lack of global alignment since there is no external tensional force to direct the alignment of the individual fibers. Moreover, the direction of neurite outgrowth is partially related to the physical shape of the EB after it has sat down on the fibrin hydrogel but overall has random directionality. After the axons reach the differentiated myofibers, at the edge of the EB's extracellular matrix, they begin to align themselves with the local direction of the myofibers. We hope to get a better understanding of neuromuscular co-localization and how the in vitro alignment matches physiologically relevant anatomy.

The use of magnetic stimulation on differentiated myofiber had little to no effect on the multitude of metrics that we collected: fiber length, width, alignment, and nuclei circularity. Despite this, we see an significant increase in these metrics when comparing the groups from an earlier to a final date. This leads us to believe that magnetic stimulation should be used at an earlier cell state to impact the metrics of differentiated muscle. Specifically, we hope to impact muscle alignment through magnetic stimulation by mechanically deforming the substrate at the myoblast stage, right after seeding. It is difficult to affect the alignment of the muscle layer after 2D differentiation. Furthermore, future work will involve querying these questions with our magnetic stimulation setup and applying it to our neuron monoculture and neuromuscular co-culture.

5. References

1. Noble J, Munro CA, Prasad VS, Midha R. Analysis of upper and lower extremity peripheral nerve injuries in a population of patients with multiple injuries. J Trauma. 1998;45: 116–122.

2. Hoben GM, Ee X, Schellhardt L, Yan Y, Hunter DA, Moore AM, et al. Increasing Nerve Autograft Length Increases Senescence and Reduces Regeneration. Plast Reconstr Surg. 2018;142: 952–961.

3. Shah HR, Bertelli JA. Long-Term Donor-Site Morbidity Following Entire Sural Nerve Harvest for Grafting. J Hand Surg Am. 2023. doi:10.1016/j.jhsa.2023.03.009

4. Bamba R, Loewenstein SN, Adkinson JM. Donor site morbidity after sural nerve grafting: A systematic review. J Plast Reconstr Aesthet Surg. 2021;74: 3055–3060.

5. Gu X, Ding F, Yang Y, Liu J. Construction of tissue engineered nerve grafts and their application in peripheral nerve regeneration. Prog Neurobiol. 2011;93: 204–230.

6. Lundborg G. Alternatives to autologous nerve grafts. Handchir Mikrochir Plast Chir. 2004;36: 1–7.

7. Xu Y, Liu Z, Liu L, Zhao C, Xiong F, Zhou C, et al. Neurospheres from rat adipose-derived stem cells could be induced into functional Schwann cell-like cells in vitro. BMC Neurosci. 2008;9: 21.

8. Osaki T, Uzel SGM, Kamm RD. On-chip 3D neuromuscular model for drug screening and precision medicine in neuromuscular disease. Nat Protoc. 2020;15: 421–449.

9. Osaki T, Uzel SGM, Kamm RD. Microphysiological 3D model of amyotrophic lateral sclerosis (ALS) from human iPS-derived muscle cells and optogenetic motor neurons. Sci Adv. 2018;4: eaat5847.

10. Cvetkovic C, Rich MH, Raman R, Kong H, Bashir R. A 3D-printed platform for modular neuromuscular motor units. Microsyst Nanoeng. 2017;3: 17015.

11. Dixon TA, Cohen E, Cairns DM, Rodriguez M, Mathews J, Jose RR, et al. Bioinspired Three-Dimensional Human Neuromuscular Junction Development in Suspended Hydrogel Arrays. Tissue Eng Part C Methods. 2018;24: 346–359.

12. Filip S, Mokrý J, English D, Vojácek J. Stem cell plasticity and issues of stem cell therapy. Folia Biol . 2005;51: 180–187.

13. Darvishi M, Tiraihi T, Mesbah-Namin SA, Delshad A, Taheri T. Motor Neuron Transdifferentiation of Neural Stem Cell from Adipose-Derived Stem Cell Characterized by Differential Gene Expression. Cell Mol Neurobiol. 2017;37: 275–289.

14. Cai C, Grabel L. Directing the differentiation of embryonic stem cells to neural stem cells. Dev Dyn. 2007;236: 3255–3266.

15. Ding Q, Edwards MM, Wang N, Zhu X, Bracci AN, Hulke ML, et al. The genetic architecture of DNA replication timing in human pluripotent stem cells. Nat Commun. 2021;12: 6746.

16. Vasyliev RG, Gubar OS, Gordiienko IM, Litvinova LS, Rodnichenko AE, Shupletsova VV, et al. Comparative Analysis of Biological Properties of Large-Scale Expanded Adult Neural Crest-Derived Stem Cells Isolated from Human Hair Follicle and Skin Dermis. Stem Cells Int. 2019;2019: 9640790.

17. Neaverson A, Andersson MHL, Arshad OA, Foulser L, Goodwin-Trotman M, Hunter A, et al. Differentiation of human induced pluripotent stem cells into cortical neural stem cells. Front Cell Dev Biol. 2022;10: 1023340.

18. Gottlieb DI. Large-scale sources of neural stem cells. Annu Rev Neurosci. 2002;25: 381–407.

19. Aydin O, Zhang X, Nuethong S, Pagan-Diaz GJ, Bashir R, Gazzola M, et al. Neuromuscular actuation of biohybrid motile bots. Proc Natl Acad Sci U S A. 2019;116: 19841–19847.

20. Webster VA, Young FR, Patel JM, Scariano GN, Akkus O, Gurkan UA, et al. 3D-Printed Biohybrid Robots Powered by Neuromuscular Tissue Circuits from Aplysia

californica. Biomimetic and Biohybrid Systems. Springer International Publishing; 2017. pp. 475–486.

21. Rousseau E, Raman R, Tamir T, Bu A, Srinivasan S, Lynch N, et al. Manuscript in revision. 2023.

22. Wichterle H, Lieberam I, Porter JA, Jessell TM. Directed differentiation of embryonic stem cells into motor neurons. Cell. 2002;110: 385–397.